Biomass Gasification for Syngas and Biochar Co-production: Energy Application and Economic Evaluation

Zhiyi Yao[1,2], Siming You[2], Tianshu Ge[3], Chi-Hwa Wang [1,2*]

[1] *Department of Chemical and Biomolecular Engineering, National University of Singapore, 4 Engineering Drive 4, Singapore 117585*

[2] *NUS Environmental Research Institute, National University of Singapore, 1 Create Way, Create Tower #15-02, Singapore 138602*

[3] *School of Mechanical Engineering, Shanghai Jiaotong University, Shanghai, China 200240*

*Corresponding author. chewch@nus.edu.sg

1. Abstract

Syngas and biochar are two main products from biomass gasification. To facilitate the optimization of the energy efficiency and economic viability of gasification systems, a comprehensive fixed-bed gasification model has been developed to predict the product rate and quality of both biochar and syngas. A coupled transient representative particle and fix-bed model was developed to describe the entire fixed-bed in the flow direction of primary air. A three-region approach has been incorporated into the model, which divided the reactor into three regions in terms of different fluid velocity profiles, i.e. natural convection region, mixed convection region, and forced convection region, respectively. The model could provide accurate predictions against experimental data with a deviation generally smaller than 10%. The model is applicable for efficient analysis of fixed-bed biomass gasification under variable operating conditions, such as equivalence ratio, moisture content of feedstock, and air inlet location. The optimal equivalence ratio was found to be 0.25 for maximizing the economic benefits of the gasification process.

Keywords: biochar; biomass gasification; energy efficiency; economics, syngas.

2. Introduction

The shortage of fossil fuel reserves and global warming sparked an eruption of research and development for renewable energy [1]. Among the plethora of renewable energy sources and technologies, thermochemical conversion of biomass is regarded to be one of feasible routes to realize a sustainable future since biomass is a carbon neutral energy source and can reduce our dependence on fossil fuels [2]. Downdraft gasification has been proved as a standout choice for small to medium size throughputs [3, 4] due to its higher efficiency as compared to other thermochemical processes such as pyrolysis, direct combustion and liquefaction [5-7].

Recently, significant attention has been paid to the numerical modelling of the gasification process which plays an important role in understanding the various physiochemical aspects of interaction within the reactor of gasification. In addition, the model could be used as a cost effective tool to predict and optimize the energy performance of gasification systems. The theoretical characterization of the four different zones in a fixed-bed gasifier and relevant reactions have been explored extensively since the early 1930s [6]. Di Blasi first proposed a complex network of reaction equations that were classified into four different gasification stages: (i) drying, (ii) pyrolysis, (iii) combustion, and (iv) reduction, with outputs being time-based axial gas composition and temperature profiles [8]. Later on, several researchers developed similar models to predict syngas composition, considering either single one stage (only reduction zone) or multi-stages of the process [9-12]. These models vary in several aspects, such as reactor configurations and reaction kinetics [13].

However, most existing models focus only on the prediction of temperature profile and syngas composition without considering biochar production[7, 11, 14-16]. Besides syngas, biochar is another valuable product from the gasification process due to its potential ability of

improving soil quality and sequestering carbon [17-19]. To predict biochar production, the heat and mass transfer on a particle level needs to be considered. Some models do consider the particle-level heat and mass transfer but they treat both solid phase and gas phase as continuous phases (which is also referred as Euler–Euler approach). This approach is appropriate only if the influential parameters (e.g., particle size, and temperature and species concentration gradient inside the particle) of a single particle on gasification performance are negligible [20]. However, it has been suggested that considering the single particle parameters and-intra-particle phenomenon can significantly improve the accuracy of gasification models in predicting important design parameters of reactor [8][21]. In this case, biomass gasification modelling should be considered as a multi-scale problem [22]; that is, the molecular level, single particle level and reactor level should all be considered. One method to solve the multi-scale problem is the Discrete Phase Model (DPM). This modelling approach treats the gas phase as quasi-continuous while each particle is tracked in a Lagrange approach. The governing equations of each particle are solved simultaneously with gas-phase balances in each time step. Several works have applied this approach to simulate the thermochemical conversion of biomass [23-25]. However, this approach is only suitable for lab-scale gasifiers with a limited number of particles due to the high computational power required [20]. An alternative method to solve solid phase with reasonable computational time is Representative Particle Model (RPM). In each cell, balance equations are solved for one representative particle and all the particles in the same cell are assumed to have the same characteristics. There are mainly two types of single particle models which could be easily coupled with the fluid phase: shrinking sphere model and shrinking core model [26, 27]. In the shrinking sphere model, the size of biomass particles reduces while their density remaining constant. The particle is assumed to be impervious with all the reaction details lumped at the gas-solid interface. As for the shrinking core model, both the size and density

of biomass particles vary. Wurzenberger coupled RPM with entire fixed-bed fluid model to simulate pyrolysis and combustion processes [28, 29]. In his work, the reactor was discretized in in the axial direction and the particle domain were discretized in the radial direction so the model was also described as 1D + 1D. Later on several research works have been conducted on multi-scale modelling of combustion and pyrolysis reactors using coupled 1D+1D model [20, 30].

In addition, there is a difference in the velocity profile between the region above air inlet and the region below air inlet. Inlet air mainly flows towards the bottom of the reactor and within this region, heat and mass transfer is dominated by forced convection. In the region above the air inlet, hot air tends to go up and the heat and mass transfer within this region is mainly controlled by natural convection. In the region near the air inlet, hot air tends to go up but pressure gradient forces the air to flow towards the bottom. These two driving forces are in the opposite direction and this special case is called mixed convection [31]. A number of studies have been conducted to investigate natural convection, forced convection and mixed convection in fixed-bed [31-34]. However, to the best of our knowledge, the application of this three-region concept (i.e. natural convection region, mixed convection region and forced convection region, respectively) on the fixed-bed modelling has not been reported.

As mentioned above, there are few gasification models which take into account both syngas and biochar production and the application of three-region modelling concept on fixed-bed gasification modelling has not been reported in the literature. In this work, we developed a coupled RPM and fixed-bed model to predict the production rate and quality of both syngas and biochar. Within each discretized cell of the reactor, one representative particle was

chosen and modelled as a shrinking sphere. The reactor was divided into three regions in terms of different fluid velocity profiles, i.e. natural convection region, mixed convection region and forced convection region, respectively. The boundary of mixed convection region was determined by sensitivity analysis. A multi-scale numerical solution procedure was adapted to solve the partial differential equations (PDEs) of molecular, particle and reactor levels. Economic evaluation was conducted taking into account economic value of syngas and biochar. The optimal equivalence ratio was found to be 0.25 for maximizing the economic benefits of the gasification process. The model could facilitate the optimization of the energy efficiency and economic viability of a gasification system, which is of significant importance to its industrial application.

3. Mathematical model

A 1-D model was developed to describe the entire fixed-bed in the moving direction z of feedstock. It was assumed that all the species were well-mixed and all the variables were uniform in the radial direction. In this model, the entire packed bed fluid model was coupled with RPM, as shown in **Figure 1**. The reactor was discretized in the z-direction and in each cell one representative particle was chosen and modelled as a shrinking sphere [26]. The reactor was divided into three regions in terms of different velocity profiles: natural convection region, mixed convection region and forced convection region. A parameter L_m was used to determine the boundary of mixed convection region. During the reaction, the biomass particle size decreased with its density being constant. The biomass particle was impervious with intra-particle diffusion and all the reaction details were lumped at the gas-solid interface. The presented model considered drying, pyrolysis, homogeneous gas reactions, and heterogeneous combustion/gasification reactions, respectively. In the gas phase eight species (O_2, N_2, CO, CO_2, H_2, H_2O, CH_4 and tar) were considered. The solid phase was woodchips. In the solid phase, all the components obtained from approximate analysis

(moisture, volatiles, fixed carbon and ash) and ultimate analysis (C, H, O, N) were treated as the dependent variables of time and space.

The conservation equations for the mass, momentum, and energy were solved for both gas phase and solid phase using the forward Euler's method. The exchange terms of momentum, mass and energy between gas phase and solid phase were treated as source terms in the conservation equations. To derive these equations, the following assumptions were made:

- The gasifier reactor is cylindrical and isotropic. The properties in both gas phase and solid phase are assumed to vary with time only along the axial direction.
- Gaseous species are assumed as ideal gases due to the low Mach number involved.
- Reactor walls are adiabatic.
- External forces such as gravity are neglected.
- There is no particle fragmentation.

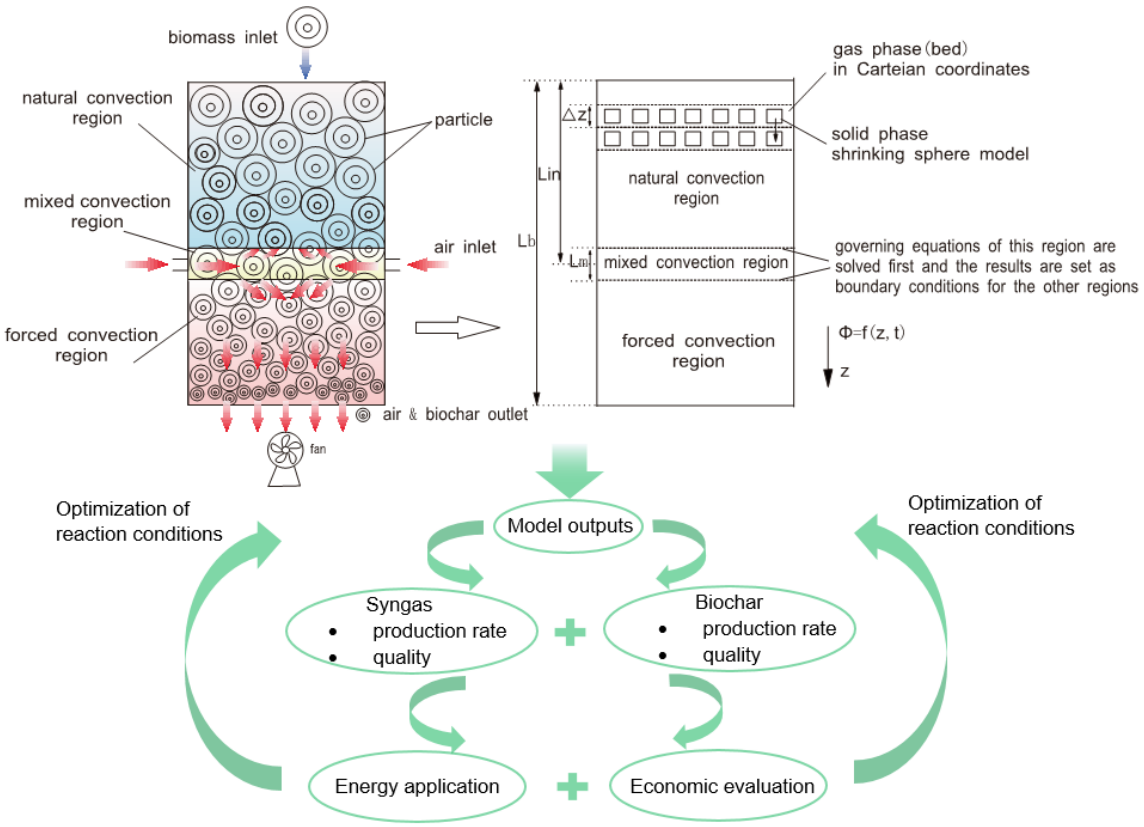

Figure 1. Modelling concept of fixed-bed down draft reactor.

3.1 Governing equations

3.1.1 Gas phase

In the gas phase, continuity equation, transient balance equations of mass, energy as well as momentum were summarized as below. All these equations were derived from the finite control volume approach, which applied balances to a cylindrical finite volume with the same radius as the gasifier reactor and an infinitesimal length.

Continuity equation in the gas phase was derived by considering the convective mass transfer and source terms of species produced in heterogeneous reactions between solid phase and gas phase:

$$\frac{\partial(\varepsilon\rho_g)}{\partial t} = -\frac{\partial(\varepsilon\rho_g u_g)}{\partial z} + \sum_i \frac{\partial}{\partial z}\left(\varepsilon\rho_g D_i \frac{\partial Y_i}{\partial z}\right) + \sum_{k,i} \varepsilon r_{vol,k}\, \upsilon_{k,i} M_i + \sum_{k,i}(1-\varepsilon) r_{suf,k}\, \upsilon_{k,i} M_i A_v \quad (1)$$

The accumulation of species i was determined by the convective mass transfer, diffusive mass transfer and source terms of species produced in homogeneous and heterogeneous reactions.

$$\frac{\partial(\varepsilon\rho_g Y_i)}{\partial t} = -\frac{\partial(\varepsilon\rho_g u_g Y_i)}{\partial z} + \frac{\partial}{\partial z}(\varepsilon\rho_g D_i \frac{\partial Y_i}{\partial z}) + \sum_k \varepsilon r_k\, \upsilon_{k,i} MW_i + \sum_k (1-\varepsilon) r_{suf,k}\, \upsilon_{k,i} MW_i A_v$$

(2)

Similarly, conductive heat transfer was neglected due to the dominance of convective heat transfer within the gas phase. In the right hand side of Eq. (2), source terms include convective heat transfer within the gas phase, convective heat transfer between the gas phase and solid phase, and heat generated from chemical reactions.

$$\rho_g \frac{\partial(\varepsilon T_g)}{\partial t} = -\frac{\partial(\varepsilon\rho_g u_g T_g)}{\partial z} - A_v(1-\varepsilon)\frac{q_{gs}}{cp_g} + \frac{\sum_k \varepsilon\rho_g r_{vol,k}\Delta H_k + \sum_k (1-\varepsilon)\rho_g A_v r_{suf,k}\Delta H_k}{\varepsilon cp_g\rho_g + (1-\varepsilon)cp_s\rho_s} \quad (3)$$

A general form of momentum balance for porous bed, Brinkman-Forchheimer equation, was applied in this work [35, 36].

$$\frac{\partial}{\partial t}(\rho_g u_g) = -\frac{\partial}{\partial z}(\rho_g u_g^2) - \frac{\partial p}{\partial z} - f_1 u_g - \varepsilon f_2 u_g^2 \quad (4)$$

where f_1 is the viscous resistance term, $f_1 = 150\frac{(1-\varepsilon)^2}{\varepsilon^3}\frac{\eta_g}{d_s^2}$, f_2 is the inertial resistance term, $f_2 = 1.75\frac{1-\varepsilon}{\varepsilon^3}\frac{\rho_g}{d_s}$. All the gaseous species were assumed as ideal gases. Heat capacity was dependent on temperature only. The ideal gas law was assumed in this model.

$$\rho_g R T_g = Mp \quad (5)$$

An empirical correlation was used to calculate the porosity as a function of particle and bed diameter in the cylindrical fixed-bed, as shown below [37]:

$$\varepsilon = 0.36 + 0.08(\frac{d_s}{d_b})^2 \quad (6)$$

3.1.2 Solid phase

Biomass particles enter the reactor from the top at velocity $u_{s,0}$. In the solid phase, a representative particle was chosen and modelled as a shrinking sphere. The shapes and aspect ratios of biomass particles do not change in the gasifier reactor, though particle sizes change dynamically. Mass balance in the solid phase was expressed in the following formula:

$$\frac{\partial}{\partial t}[\frac{1}{3}\rho_s(\frac{d_s}{2})^3] = \sum_{k,j} r_{suf,k}\, \upsilon_{k,j} M_j (\frac{d_s}{2})^2 \quad (7)$$

Initially, wood was represented by the maximum yield of moisture, volatile, fixed carbon and ash based on the results of the approximate analysis. Solid compositions were calculated by atomic balance equations:

$$\frac{\partial}{\partial t}[\frac{1}{3}\rho_s(\frac{d_s}{2})^3 Y_j] = \sum_k r_{suf,k}\upsilon_{k,j}\, M_j \left(\frac{d_s}{2}\right)^2 \quad (8)$$

It was assumed that the gas, liquid, and solid phases of a particle had the same local temperature. An overall energy equation was expressed as:

$$\frac{\partial T_s}{\partial t} = A_v \frac{q_{gs}}{\rho_s c_{ps}} - \frac{1}{\rho_s c_{ps}} \frac{\partial q_{ss}}{\partial z} + \frac{\sum_k \varepsilon r_{vol,k} \Delta H_k + \sum_k (1-\varepsilon) A_v r_{suf,k} \Delta H_k}{\varepsilon c_{pg} \rho_g + (1-\varepsilon) c_{ps} \rho_s} \quad (9)$$

The inter-phase heat exchange was assumed to be dependent on the temperature difference between the solid phase and gas phase, including convective and radiative heat transfer:

$$q_{gs} = h_{gs}(T_g - T_s) + \sigma\epsilon(T_g^4 - T_s^4) \quad (10)$$

Conductive heat transfer in solid phase was calculated as:

$$q_{ss} = -\kappa \frac{\partial \mathrm{T}_s}{\partial \mathrm{z}} \quad (11)$$

The velocity of biomass particle depends on the feeding rate of feedstock:

$$u_s = \frac{4F_s}{(1-\varepsilon)\rho_s \pi d_b^2} \quad (12)$$

3.2 Reaction models

3.2.1 Drying

The drying process was classified into two stages in terms of the particle temperature. When the particle temperature is below the boiling temperature of water, the drying is controlled by the concentration difference of water between surrounding air and particle. After reaching boiling temperature, evaporation occurs at isothermal conditions and all incoming thermal flux is consumed for water vaporization [38]. The water content in the biomass is broken down into free and bound water. A summary of the mathematical formulation used to describe the water mass flux during drying is detailed in **Table 1**.

$$F_w = -F_{free,w} - F_{bound,w} \quad (13)$$

Table 1. Governing equation for the drying process.

		Free Water	Bound Water
T_p T_{evap}	<	$F_{m,w}^{free,Tp} = 4\pi r^2 k_m(\rho_w^{sat} - \rho_w^{\infty})$	$F_{m,w}^{bound,Tp} = 4\pi r^2 k_m(\rho_w^{vap} - \rho_w^{\infty})$
T_p T_{evap}	=	$F_{m,w}^{free,Tevap} = \frac{Q_{gs}}{\Delta H_w^{vap}}$	$F_{m,w}^{bound,Tevap} = \frac{Q_{gs}}{\Delta H_w^{vap} + \Delta H_w^{des}}$

3.2.2 Pyrolysis

A two-step model was used to simulate pyrolysis process, in which biomass undergoes primary pyrolysis followed by tar cracking reactions [12].

Primary pyrolysis: $volatile \rightarrow 0.268\mathrm{CO} + 0.295\mathrm{CO_2} + 0.094\mathrm{CH_4} + 0.5H_2 + 0.255H_2O + 0.004NH_3 + 0.0002\mathrm{H_2S} + 0.2\text{primary tar}$ (r_{p1})

Tar cracking:

$primary\ tar \rightarrow 0.261\text{secondary tar} + 2.6\mathrm{CO} + 0.441\mathrm{CO_2} + 0.983\mathrm{CH_4} + 2.161H_2 + 0.408\mathrm{C_2H_4}$ (r_{p2})

The reaction rates are calculated by:

$r_{p1} = 4.38 \times 10^9(1-\varepsilon)\exp\left(\frac{-1.527\times10^5}{RT_s}\right)C_{volatile}.$

$r_{p2} = 4.28 \times 10^6\varepsilon \times \exp\left(\frac{-1.08\times10^5}{RT_g}\right)C_{primary\ tar}.$

Chemical formula of the primary tar was expressed as $C_{6.407}H_{11.454}O_{3.482}$ and the secondary tar was assumed to be pure benzene [39]. The compositions of the product gas from the primary pyrolysis [40] and tar cracking [41] reactions were estimated on the basis of the literature data for wood.

3.2.3 Biochar reactions

To determine the overall reaction rate, both kinetics reaction rate and film mass-transfer diffusion were considered at the gas-solid interface [12]. The surface reaction rate was calculated by:

$$r_{suf,k} = \left(\frac{1}{v_i MW_i}\right) \frac{\rho_i}{\frac{1}{s_k} + \frac{1}{r_{s,k}}} \quad (14)$$

All the heterogeneous reactions considered in this model were summarized in **Table 2**. The film diffusion rate for the mixed and forced convection region was determined using: [42]

$s_k = \frac{2.06G}{(1-\varepsilon)\rho_g} Re^{-0.575} Sc^{-2/3}$ and $s_k = Sh \times D/L^*$, respectively.

Table 2. Heterogeneous biochar reactions.

	reactions	kinetic reaction rate(m/s)	reference
RS1	$2C + O_2 \xrightarrow{r_{s1}} 2CO$	$r_{s1} = 2.3T_s \exp(-11100/T_s)$	[43]
RS2	$2C + O_2 \xrightarrow{r_{s2}} CO_2$	$\frac{r_{s1}}{r_{s2}} = 2512\exp(-6420/T_g)$	[44]
RS3	$C + H_2O \xrightarrow{r_{s3}} CO + H_2$	$r_{s3} = 5.714T_s \exp(-15600/T_s)$	[45]
RS4	$C + CO_2 \xrightarrow{r_{s4}} 2CO$	$r_{s4} = 589T_s \exp(-26800/T_s)$	[46]
RS5	$C + 2H_2 \xrightarrow{r_{s5}} CH_4$	$r_{s5} = 3.42 \times 10^{-3} T_s \exp(-15600/T_s)$	[47]

3.2.4 Homogeneous reactions

Gaseous species including CO_2, CO, H_2O, H_2, CH_4, O_2, N_2 were considered in this model. All the kinetic rates of homogeneous reactions are listed in **Table 3**. The overall reaction rates are equal to the minimum value of turbulent mixing rates and kinetics reaction rates [12].

$$r_{vol,k} = \min(r_{g,k}, r_{tm,k}) \quad (15)$$

where $r_{tm,k}$ was expressed using Eddy Dissipation Model (EDM):

$$r_{tm,k} = 4\rho_g \frac{\epsilon_t}{\kappa} \min\left(\frac{Y_i}{v_i M_i}, \frac{Y_j}{v_j M_j}\right) \quad (16)$$

Table 3. Homogeneous reactions.

	reactions	kinetic reaction rate (kmol $m^{-3}s^{-1}$)	reference
RG1	$\text{pri tar} + O_2 \xrightarrow{r_{g1}} H_2O + CO$	$r_{g1} = 59.8 T_g p^{0.3} \varepsilon \exp(-12200/T_g) C_{pritar}^{0.5} C_{O_2}$	[46]
RG2	$\text{sec tar} + O_2 \xrightarrow{r_{g2}} H_2O + CO$	$r_{g2} = 59.8 T_g p^{0.3} \varepsilon \exp(-12200/T_g) C_{sectar}^{0.5} C_{O_2}$	[46]
RG3	$H_2 + \frac{1}{2}O_2 \xrightarrow{r_{g3}} H_2O$	$r_{g3} = 3.53 \times 10^{8.4} \varepsilon \exp(-3670/T_g) C_{H_2}^{1.1} C_{O_2}^{1.1}$	[48]
RG4	$\text{CO} + \frac{1}{2}O_2 \xrightarrow{r_{g4}} CO_2$	$r_{g4} = 1.3 \times 10^{11} \varepsilon \exp(-15105/T_g) C_{CO} C_{H_2O}^{0.5} C_{O_2}^{0.5}$	[49]
RG5	$\text{CO} + H_2O \xrightarrow{r_{g5}} H_2 + CO_2$	$r_{g5} = 2.78\varepsilon \exp\left(-\frac{1511}{T_g}\right)[C_{CO} C_{H_2O} - \frac{\exp\left(-\frac{7914}{T_g}\right) C_{CO_2} C_{H_2}}{0.0265}]$	[45, 50]
RG6	$CH_4 + 1.5O_2 \xrightarrow{r_{g6}} CO + 2H_2O$	$r_{g6} = 1.0 \times 10^{11.7} \varepsilon \exp(-24357/T_g) C_{CH_4}^{0.7} C_{O_2}^{0.8}$	[51]
RG7	$CH_4 + H_2O \xrightarrow{r_{g7}} CO + 3H_2$	$r_{g7} = 3.0 \times 10^{8} \varepsilon \exp(-15083/T_g) C_{CH_4} C_{H_2O}$	[52]

3.3 Heat and mass transfer coefficient in each region

3.3.1 Mixed convection region

The air inlet locates at the mixed convection region. Uniform plug flow is assumed at the air inlet with 79% N_2 and 21% O_2, temperature T_0, and velocity u_0. In this region the fluid (gaseous mixture) flows in a "turbulent manner". Due to the complex flow patterns and fluid dynamics near the air inlet, this region was modelled as a black box where all the variables distribute evenly along the axis direction, which meant all the terms regarding spatial variation in the governing equations of gas phase were ignored. To calculate the heat transfer coefficient, the Nusselt number was determined by the following formula [31]:

$$Nu_m = (Nu_n^3 + Nu_f^3)^{1/3} \quad (17)$$

In addition, the governing equations of this region were solved first and the results were set as boundary conditions for the next two regions.

3.3.2 Natural convection region

In the natural convection region, the temperature difference is the main driving force for both heat and mass transfer. The heat transfer coefficient between two phases h_{gs} was dependent on Nu_n, which can be obtained from Ra_n:

$$h_{gs} = \frac{\kappa_g Nu_{n,d_s}}{d_s} \quad (18)$$

$$Nu_{n,ds} = 2 + 0.43Ra_{n,ds}^{1/4} \quad (19)$$

$$Ra_{n,ds} = Gr \cdot \Pr = \frac{\beta g \rho^2 d_s^3 \Delta T}{\mu^2} \cdot \frac{\mu c_{pg}}{\kappa_g} \quad (20)$$

In the gas phase, the convection term $-\frac{\partial(u_g T_g)}{\partial z}$was replaced by $-\frac{h_{gg}\varepsilon}{c_{ps}\rho_s}\frac{\partial T}{\partial z}$, where the heat transfer between two discretized volumes was calculated using the horizontal hot plate model:

$$h_{gg} = \frac{\kappa_g Nu_{n,L^*}}{L^*} \quad (21)$$

$$Nu_{n,L^*} = 0.54Ra_{n,L^*}^{\frac{1}{4}} \qquad 10^5 < Ra_{n,L^*} < 2 \times 10^7$$

$$Nu_{n,L^*} = 0.14Ra_{n,L^*}^{\frac{1}{3}} \qquad 2 \times 10^7 < Ra_{n,L^*} < 3 \times 10^{10} \quad (22)$$

$$Ra_{n,L^*} = Gr \cdot \Pr = \frac{\beta g \rho^2 {L^*}^3 \Delta T}{\mu^2} \cdot \frac{\mu c_{pg}}{\kappa_g} \quad (23)$$

where L^* is the characteristic length, $L^* = \frac{Area}{perimeter} = \frac{\pi r_b^2}{4\pi r_b} = \frac{r_b}{4}$

In addition, it was assumed that diffusion dominated in this region so that the convection term of species balance equation was neglected. For all the scalar variables, Dirichlet boundary conditions were used at $z = L_{in} - \frac{L_m}{2}$, whereas Neumann conditions were used at z = 0.

3.3.3 Forced convection region

In the forced convection region, the pressure difference is the main driving force for both heat and mass transfer. The heat transfer coefficient h_{gs} is determined by Nusselt number according tothe convective heat transfer mechanism within the fixed-bed reactor [53].

$$Nu_f = 2 + 1.1Pr^{1/3}Re^{0.6} \quad (24)$$

In this region, uniform plug flow with velocity $u|_{z-}$ was assumed at $z = L_{in} + \frac{L_m}{2}$, and atmospheric pressure was assumed at the reactor outlet. For all the other scalar variables, Dirichlet boundary conditions were used at $z = L_{in} + \frac{L_m}{2}$, whereas Neumann conditions were used at $z = L_b$.

3.4 Numerical solution procedure

To solve the governing equations, finite volume scheme was used for discretization. Cylindrical grid that has the same radius as the gasifier reactor and length Δz was used to describe the gasifier reactor domain. In each volume, a representative particle was chosen and modelled as a shrinking sphere, moving towards the bottom of the reactor. The velocity profile was specified at cell edges and the scalar variables were specified at cell centers. Usually the unsteady reactive flow problems are solved by fractional step methods or similar methods such as PISO (Pressure Implicit with Splitting of Operator) [54-57], because the pressure correction equation (in multi-scale reactor models also the particle model) is solved just once per time step. The solution algorithm is an extension of the algorithm introduced by Jakoben's group [20, 55, 56].

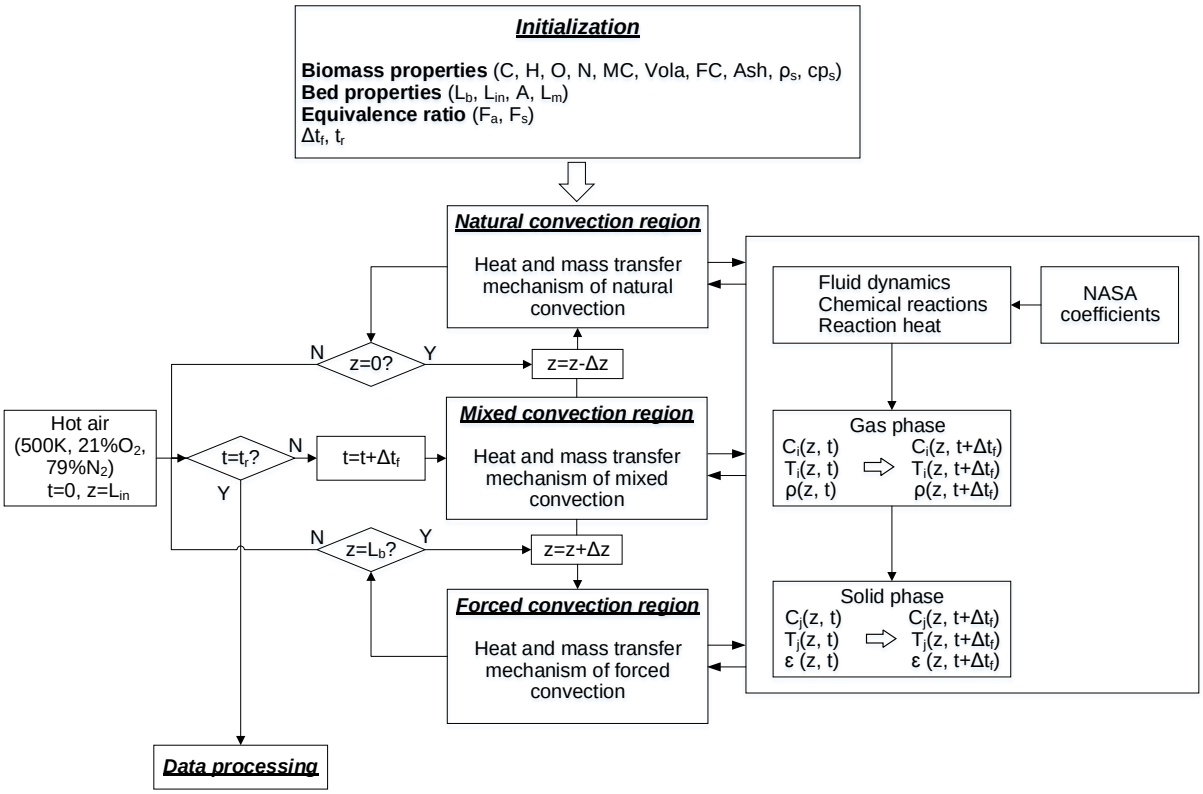

Figure 2. Structure of simulation procedure.

The detailed structure of the simulation procedure is shown in **Figure 2**. The governing equations of mixed region were solved first and the results were set as boundary conditions for the other regions. After Δt, all the properties $\varphi(z,t)$ in gas phase and solid phase were updated to $\varphi(z,t+\Delta t)$. In addition, to solve energy balance equations, NASA coefficients were used to calculate reaction heat [58]. In this study, the simulation program was coded in MATLAB R2014a. All the model inputs, number of grids and time steps were summarized in **Table 4**.

Table 4 Model inputs and parameters [38] [59].

Results of ultimate analysis	C	44%
	H	6%
	O	48%
	N	2%
Results of approximate analysis	water	8%
	volatiles	68%
	fixed carbon	17%
	ash	7%
Characteristics of gasifier reactor	L (Total length of gasifier reactor, m)	0.5
	L_a (Length of the region above gasifier reactor, m)	0.25
	A_c (Cross sectional area of gasifier reactor, m^2)	0.07
	ε (Porosity of fixed-bed)	0.4
	Biomass resident time, min	30
Physical properties of biomass particle	cp_s(specific heat capacity of biomass particle, J kg^{-1} K^{-1})	1350
	ρ_b (biomass particle density, kg m^{-3})	830
	ΔH_w^{vap} (enthalpy of vaporization, J kg^{-1})	$\Delta H_w^{vap} = 28.92 \times 10^5 (1 - \frac{T_p}{647.13})^{0.32 - 0.212\left(\frac{T_p}{647.13}\right) + 0.26(T_p/647.13)^2}$
	ΔH_w^{des} (enthalpy of desorption, J kg^{-1})	$\Delta H_w^{des} = \exp(13.71 - 31.90 Y_{water})$
	k_{ss}(heat conductivity of biomass particle, W $m^{-1}K^{-1}$)	0.08
	ρ_w^{sat} (water mass concentration at the surface of the particle in saturated air conditions, kg m^{-3})	$\rho_w^{sat} = \exp(73.56 - \frac{7258.2}{T_f} - 7.3 log T_f + 4.16 \times 10^{-6} {T_f}^2)$
	a_w (water activity)	$a_w = 1 - \exp(-5.85 T_f^{0.442} Y_{water}^{14.23 T_f^{-0.3953}})$
	ρ_w^{vap} (water mass concentration at the surface of the particle in non-saturated conditions (kg m^{-3})	$\rho_w^{vap} = a_w \times \rho_w^{sat}$
Physical properties of gaseous species	cp_g (specific heat capacity, J $kg^{-1}K^{-1}$)	$cp_g = 1053.92 - 0.3993 T_g + 9.547 \times 10^{-4} T_g^2 - 5.732 \times 10^{-7} T_g^3 + 6.991 \times 10^{-11} T_g^4$
	η (dynamic viscosity, 10^{-5}Pa s^{-1})	$\eta = -0.00122 + 0.00797 T_g - 7.44593 \times$

		$10^{-6}T_g^2 + 5.1782 \times 10^{-9}T_g^3 - 1.54468 \times 10^{-12}T_g^4$
	k_g (heat conductivity, W $m^{-1}K^{-1}$)	$k_g = 3.14 \times 10^{-4}T_g^{0.78}/(1 - \frac{0.71}{T_g} + \frac{2121.7}{T_g^2})$
	D (diffusivity, m^2 s^{-1})	$D = 3 \times 10^{-5}$
Time step	Δt	10^{-3}s
	t_r*	2 hours
Finite volume length	Δz	0.01m

*Gasification time was set as 2 hours. The model could reach steady state within 2 hours gasification running time.

3.5 Equivalence ratio (ER), higher heating value (HHV) and cold gas efficiency (CGE)

In order to encapsulate the effects of both air flow and biomass feeding rates, the ER is defined as [60]:

$$ER = \left(\frac{F_{air}}{F_s}\right) / \left(\frac{F_{air}}{F_s}\right)_{Stoichiometric} \quad (25)$$

where F_{air} is the inlet air mass flow rate (kg/s), F_s is the biomass feeding rate (kg/s). The CGE could be used to indicate gasifier efficiency and is defined as the ratio of energy of the producer gas to the energy of the consumed biomass [61].

$$\boldsymbol{CGE = \frac{HHV_g \times F_g}{HHV_s \times F_s}} \quad (26)$$

where HHV_g is the higher heating value of syngas ($MJ\ Nm^{-3}$), F_g is the syngas production rate ($kg\ s^{-1}$), HHV_s is the higher heating value of biomass, F_s is the feedstock feeding rate ($kg\ s^{-1}$).

HHV of feedstock and biochar was calculated based on the empirical correlation developed by Channiwala SA et.al [62].

$$HHV_s = 0.349C + 1.178H + 0.101S - 0.103O - 0.015N - 0.021A \quad (27)$$

where $C, H, S, O, N\ and\ A$ represent carbon, hydrogen, sulphur, oxygen, nitrogen, and ash content of material, respectively, expressed in mass percentage on dry basis.

3.6 Economic value of biochar and syngas

Syngas and biochar are two main products from the gasification process and both of them have considerable economic values. However, there are still limited studies that evaluate the overall economic benefit in terms of both syngas and biochar production.. The total economic value Vof the gasification products is expressed as the following:

$$V = P_c \times R_c + P_g \times R_g \tag{28}$$

Where P_c is the unit price of biochar, \$/kg; R_c is the production rate of biochar kg/kg feedstock; P_g is the unit price of syngas, \$/Nm^3; R_g is the production rate of syngas Nm^3/kg feedstock. The unit prices of produced biochar and syngas were obtained from literatures, which are expressed as the following

$$P_C = f_c \times HHV_C \tag{29}$$

$$P_g = f_g \times HHV_g \tag{30}$$

Where f_c is the price of biochar per mega joule [63], $f_c = 2.528 \times 10^{-3} \$/MJ$. HHV_C is the higher heating value of biochar, MJ/kg, f_g is the price of syngas per mega joule [64], $f_g = 6.78 \times 10^{-3}\ \$/MJ$. HHV_g is the higher heating value of syngas, MJ/Nm^3.

4 Results and Discussion

4.1 Model validation

Experimental results were obtained from our group's previous gasification experiments[11]. The experiments were conducted using a GEK fixed-bed downdraft gasifier manufactured by All Power Labs. The gasifier has a capacity of 10kg/h and its geometrical parameters are listed in **Table 4**.

Sensitivity analysis was performed by varying the length of mixed convection region L_m. The results are shown in **Table 5**. The standard deviation (SD) between the experimental and simulation results was defined as: $SD = \sqrt{\frac{\sum_n (r_s - r_e)^2}{n-1}}$, where r_s and r_e represent simulation results and experimental results, respectively. From the table we can see that the SDs across different gaseous species was 3.1, 3.04, 3.02, 3.01, 3.03, and 4.17 at L_m/L_b ratio equalling 0.02, 0.04, 0.06, 0.08 and 0.1, respectively. The length of mixed convection region had a relatively small influence on the model prediction within the range from 0.02 to 0.1, while there was an obvious increase of SD from 3.03 to 4.17 with the length ratio further increasing from 0.1 to 0.2. The SD reached its minimum when the length ratio equals 0.08. The minimum average SD was 3.01 at L_m/L_b = 0.08 and length ratio was chosen as one of the model inputs for further analysis. The results show this three-region modelling concept is appropriate to describe the fixed-bed downdraft gasification process.

Table 5 Comparison of predicted syngas composition under different length of mixed convection region.

			L_m/L_b					
			0.02	0.04	0.06	0.08	0.1	0.2
Syngas composition (vol%)	N_2	45.62	48.47	48.47	48.63	48.63	48.8	50.42
	CO	15.91	16.94	16.94	16.92	16.92	16.90	16.65
	H_2	17.78	15.25	15.24	15.14	15.12	14.98	13.49
	CH_4	2.01	2.54	2.54	2.54	2.54	2.53	2.50
	CO_2	12.62	16.79	16.81	16.78	16.79	16.77	16.94
	O_2	2.12	0	0	0	0	0	0
	C_nH_m	3.94	0	0	0	0	0	0
Biochar composition	C	85.77	79.63	79.64	79.66	79.67	79.69	77.35
	H	1.52	1.04	1.64	2.12	2.45	2.45	2.60

(vol%)	O	12.21	15.61	15.6	15.59	15.58	15.56	18.77
	N	0.5	3.58	2.94	2.42	2.06	2.02	0.80
	S	0	0.14	0.18	0.21	0.24	0.28	0.48
	SD		3.10	3.04	3.02	3.01	3.03	4.17

The temperature and particle mass distributions along the axis direction of the gasifier were predicted with the fixed length (L_m/L_b) of 0.08 for the mixed convection region, as shown in **Figure 3**. The temperature distribution inside the gasifier was affected by the ER. It was found that the temperature at all locations of the gasifier increased with the increase of ER. This is due to the fact that the higher air flow rate promotes the exothermic combustion reactions. More reaction heat is generated and hence the temperature inside the gasifier increases. Moreover, the temperature reached its peak in the mixed convection region near the air inlet. The highest temperature was 1030, 1069, 1235^{o}C based on the model prediction and 920, 998, 1131^{o}C based on the experimental data under the condition of ER=0.35, 0.6, 0.85, respectively. This is because energy is generated by exothermic combustion reactions in this region. After oxygen was depleted, pyrolysis and endothermic reduction reactions dominate. Correspondingly, the mass reduction rate of biomass particle is closely related to the gaseous species concentration and the temperature distribution profile inside the reactor. In the natural convection region, there is a fast mass loss for biomass particles since volatiles are released by pyrolysis reactions. In the mixed convection region, which is near the air inlet, the heterogeneous reactions between carbon and gaseous species take place quickly leading to higher temperature and higher oxygen concentration. In addition, it was noted that there was a similar trend for the particle mass change across the different ER conditions and the particle mass decreased with the increase of ER.

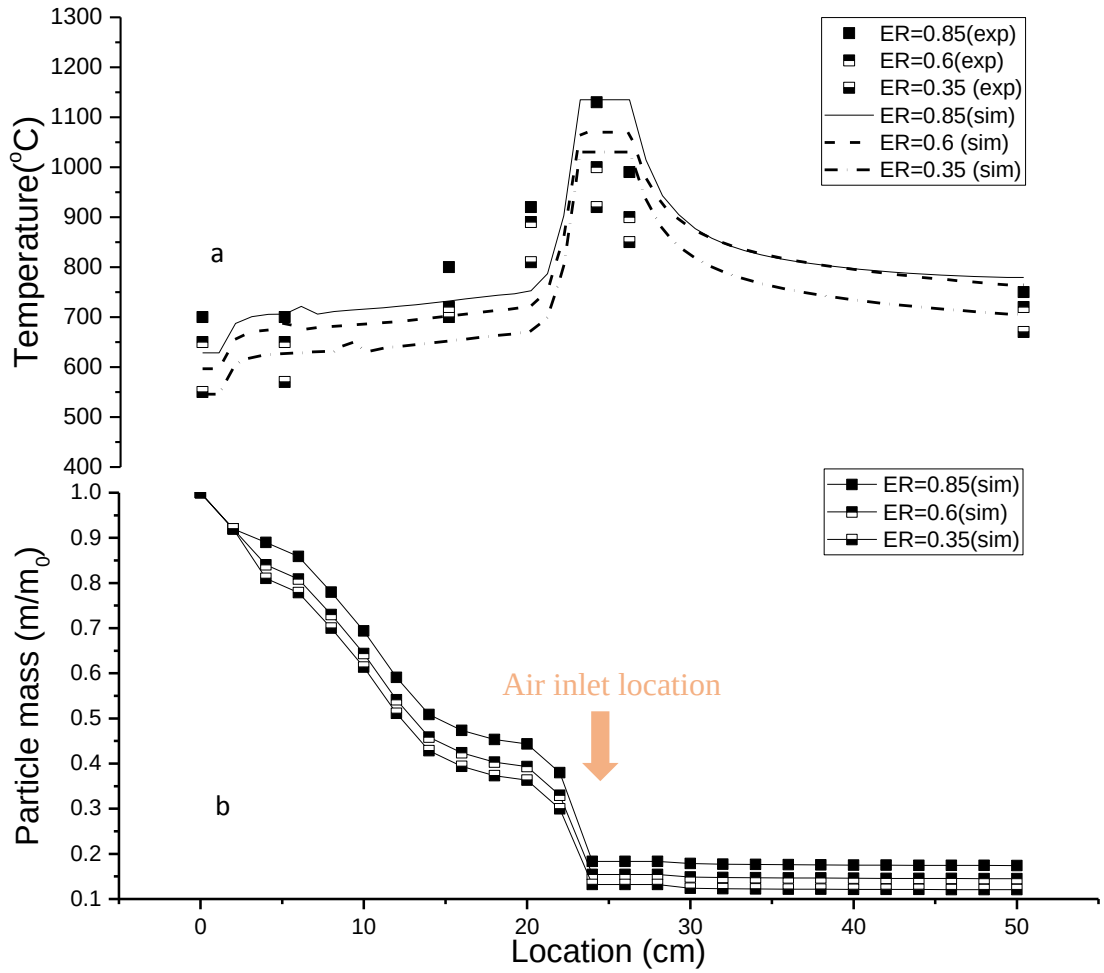

Figure 3a Temperature distribution along the axis direction under different ER.

Figure 3b Particle size distribution along the axis direction under different ER.

4.2 Effects of ER on syngas production rate and its quality

The effects of ER on syngas production rate and CGE are shown in **Figure 4**. The CO_2 content and H_2 content in the producer gas decreased from 27.78% to 8.10% and 25.02% to 9.00%, respectively as ER increased from 0.1 to 0.6. Since biochar gasification reactions with CO_2 and steam are endothermic, they are favored at relatively high temperatures [65]. Increasing ER leads to the increase in temperature, which promotes the reverse water-gas shift reaction and decreasesH_2 and CO_2 concentrations. This finding is also in a good agreement with the literature [66]. The HHV of the producer gas decreased from 6.15 to 3.60

MJ/Nm^3 as ER increased from 0.1 to 0.6. This is because 1) the significant decrease in H_2 and CH_4 concentrations in the producer gas; 2) the inert N_2 did not contribute to the HHV of syngas and its fraction increased with increasing ER. This result is consistent with the previous works done by Sheth and Babu [9] and Seggiani et al [67], who observed the decrease of HHV when the ER increased. Both HHV of syngas and its production rate contribute to the CGE and their combined effects on the CGE were evaluated by plotting CGE against ER. It was found that the CGE first increased with increasing ER from 0.1 to 0.25 and then dropped to 61.25% at ER of 0.6. The maximum CGE was 72.75% at ER= 0.25. The numerical values of the optimum ERs and maximum CGE are presented below in **Table 6**, together with data procured from experiments conducted in other studies.

Table 6. Comparison of simulation with literature.

Source	Biomass Type	Optimum Equivalence Ratio	CGE
Dogru et al. [68]	Hazelnut Shells	0.28	80.91
Zainal et al. [69]	Furniture wood and charcoal	0.39	33.72
Sheth & Babu [9]	Furniture waste	0.20	56.87
This work	100% Wood Chips	0.25	72.75

In this work, for a biomass sample of 100% wood chips, the optimum ER was 0.25 which led to a CGE of 72.75%. In Dogru et al.'s [68] study, an extremely high CGE of 80.91% was found for a relatively small equivalence ratio. On the other hand, Zainal et al. only manages to achieve a CGE of 33.72% with a relatively high equivalence ratio of 0.39. Two main reasons could account for this difference. Firstly, it could be hypothesized that hazelnuts offer a better alternative to furniture wood and charcoal as a biomass gasification choice due to its favourable elemental compositions. Another possible explanation could stem from the use of

different gasifiers. Dogru et al. made use of a pilot scale fixed-bed downdraft gasifier with a diameter ranging from 135mm to 450mm and a total height of 0.81m [68], Zainal et al. utilized a blow-type downdraft gasifier with a cone structure with a main body diameter of 600mm and total height of 2.5m [69].

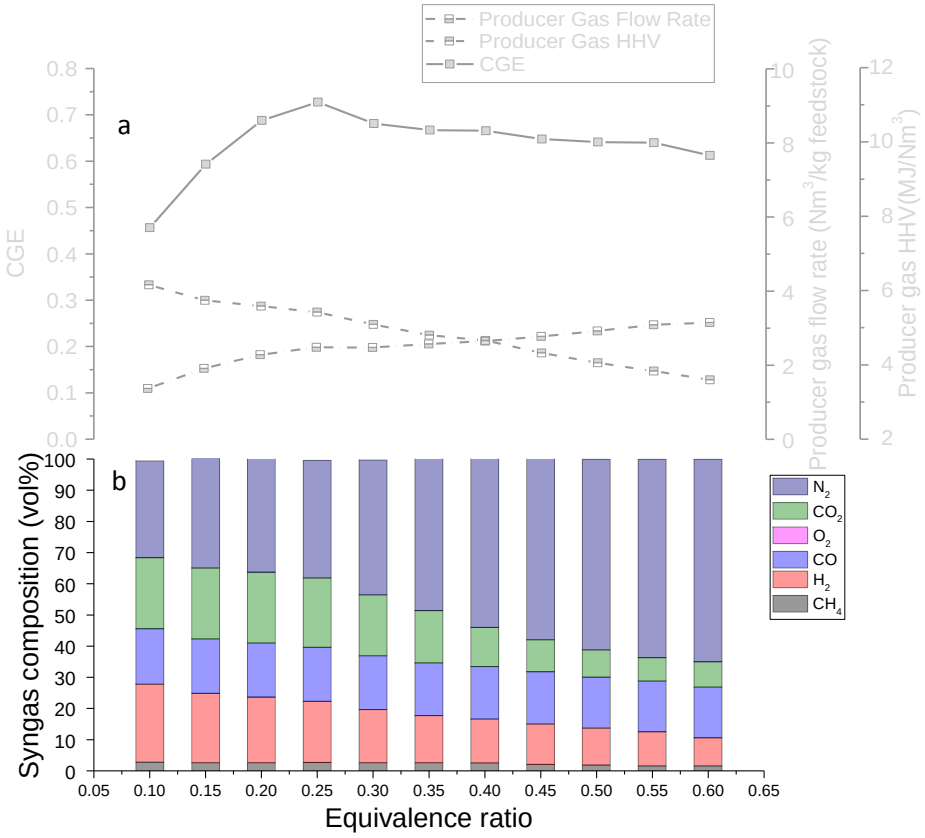

Figure 4a: Effects of ER on producer gas flow rate, producer gas HHV, and CGE;
Figure 4b: Effects of ER on producer gas composition

4.3 Effects of ER on biochar production rate and its quality

In an industrial gasification plant, biochar could be sold as barbecue materials and fertilizer after treatment [71, 72]. The quality of produced biochar is closely related to its carbon content [73]. However, to the authors' best knowledge, most models focus only on the prediction of syngas composition without considering biochar production. In this model biochar is defined as a mixture of bottom biochar and ash produced from a fixed-bed downdraft gasification system. **Figure 5** shows the effects of ER on the production rate and the quality of biochar. With increasing ER, more oxygen is fed into the reactor, speeding up

the heterogeneous reactions to convert more carbon from solid phase into gaseous species. Henceforth, the carbon content of the produced biochar decreased from 88.17% to 71.16% as ER increased from 0.1 to 0.6. The similar trend was observed in the biochar production rate, which decreased from 0.22 kg/kg biomass to 0.14 kg/kg biomass as ER increased from 0.1 to 0.6. The trend of both carbon content of biochar and its production rate indicate that the total amount of carbon in biochar decreased with increasing ER, which means the increase of ER has negative effects on the quality and production rate of biochar. The results agree with the work by Meyer S et al [71], which reported that the biochar production rate from gasification is around 10%.

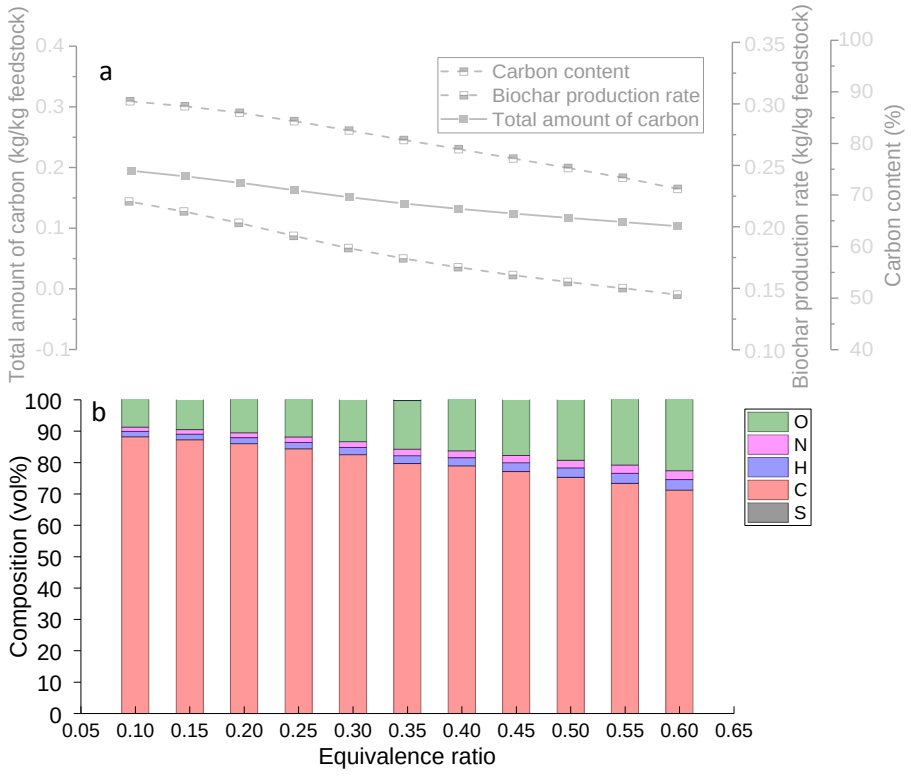

Figure 5a: Effects of ER on carbon content, biochar production rate, and total amount of carbon;
Figure 5b: Effects of ER on biochar composition

4.4 Evaluation of economic benefits

Figure 6 shows the overall economic benefits based on the production rate and quality of both syngas and biochar predicted by the model. As ER increased from 0.1 to 0.6, the carbon

content in biochar decreased due to the speed up of heterogeneous reactions with the existence of more oxygen, which further led to the decrease of biochar prices from 0.017$/kg feedstock to 0.009$/kg feedstock. However, with increasing ER the syngas price showed similar trend with its CGE. It first increased from 0.057$/kg feedstock to 0.091$/kg feedstock as ER increased from 0.1 to 0.25 and then dropped to 0.077 $/kg feedstock at ER=0.6. By considering the contributions of both syngas and biochar, the optimum ER was found to be 0.25 in terms of economic benefits of the gasification process. The maximum economic benefit could reach 0.11 $/kg feedstock based on the model prediction. The results could facilitate the optimization of the energy efficiency and economic viability of a gasification system, which is of significant importance to its industrial application.

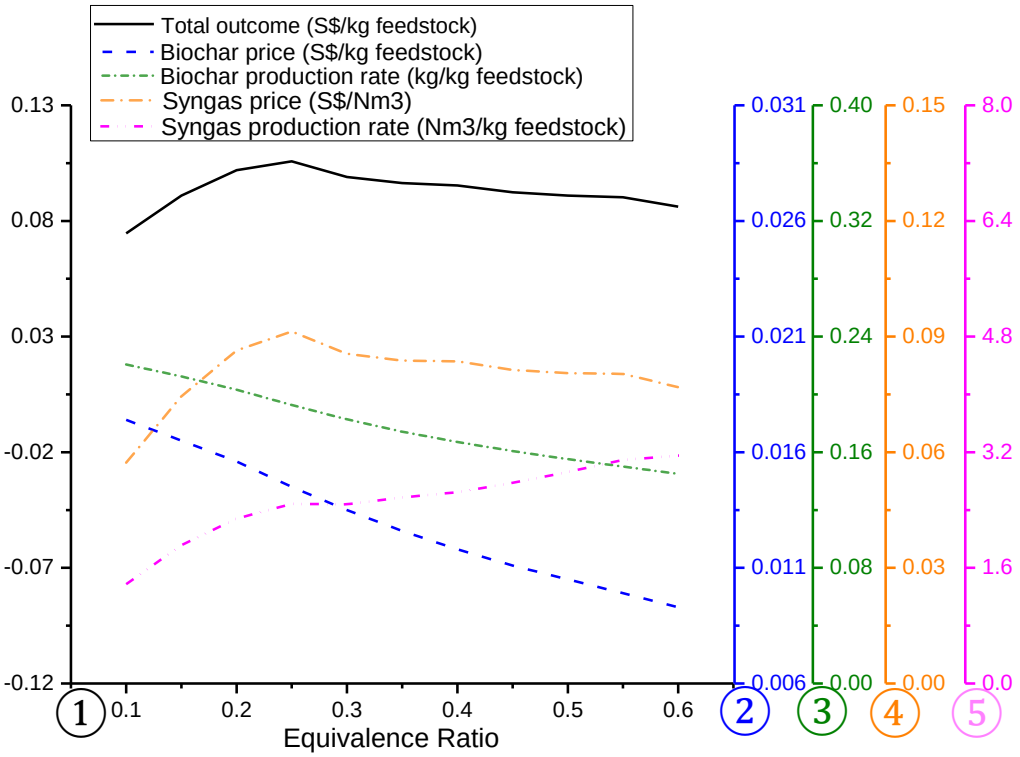

Figure 6 Evaluation of overall economic benefits.

4.5 Effects of moisture content on syngas composition and reaction temperature

To investigate the effects of moisture content on producer gas quality, the simulation was conducted at the optimal ER of 0.25 under different moisture contents (0-30%) of the feedstock. The results are shown in **Figure 7**. From the figure we can see that when the moisture content increased from 0 to 0.3 the volume fraction of CO_2, H_2, and HHV of syngas increased from 20.45%, 18.09%, and 5.39 MJ/Nm^3 to 27.12%, 23.99%, and 5.48 MJ/Nm^3, respectively. Conversely, the volume fraction of CO decreased from 18.67% to 13.49%. In addition, produced syngas temperature decreased from 992.3K to 834.6K as the moisture content increased from 0 to 0.3, due to the fact that the increase of moisture content causes more energy consumption for evaporation.

The volume fractions of H_2 and CO_2 increased as the increase of moisture content because the increasing moisture content favours reactions RS3 (Table 2) and RG5 (Table 3) to produce more H_2 and CO_2. Reaction RS1 (Table 2) is a heterogeneous reaction between gas phase and solid phase, but reaction RG4 (Table 3) and RG5 (Table 3) are homogeneous reactions in the gas phase. Henceforth, the consumption rate of CO in homogeneous reactions is higher than the production rate in the heterogeneous reaction. This would lead to a decrease in CO concentration with the increasing moisture content. Although the CO concentration decreased with increasing moisture content of feedstock, the HHV of syngas still increased due to the increasing concentrations of CH_4 and H_2. The same trends were observed in the experiments conducted by Xie and colleagues [74].

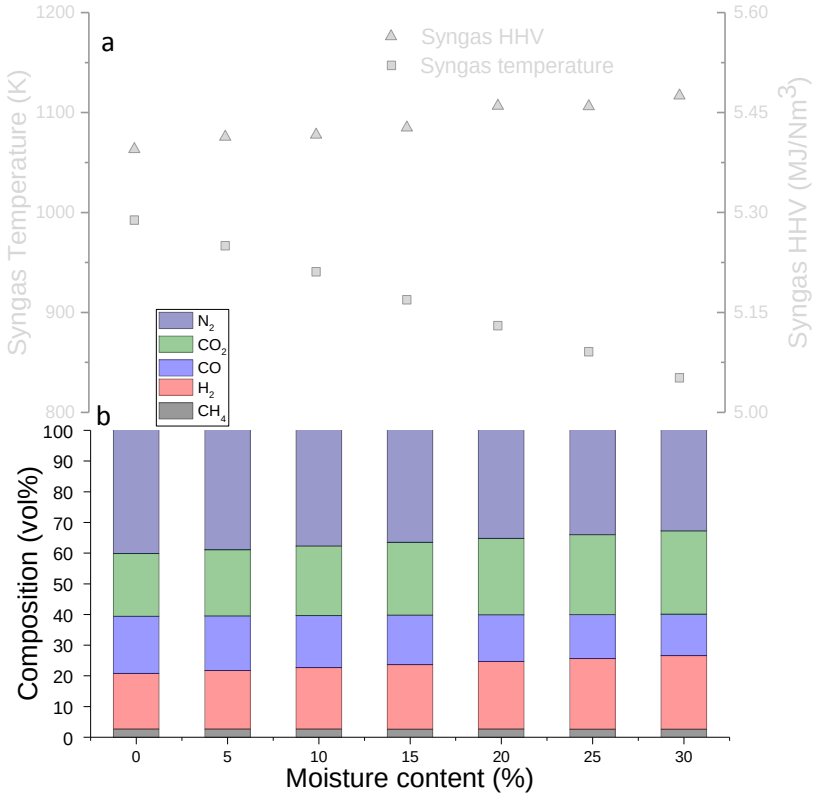

Figure 7a; Effects of moisture content on syngas temperature and syngas HHV;
Figure 7b: Effects of moisture content on syngas composition.

4.6 Effects of air inlet location on the gasification performance

This model could facilitate the design of gasifier reactor by providing an insight into the effects of air inlet location on the temperature profile, syngas production, and biochar production. The results are shown in **Figure 8.** In this session, La/L is the ratio of the length of the region above air inlet to the total length of the reactor. **Figure 8a** shows the effects of air inlet location on syngas composition and its HHV. There was no significant variation of CO and CH_4 within the range of La/L from 0.2 to 0.8. However, the volume concentration of H_2 increased from 8.19% to 20.41% as La/L increased from 0.2 to 0.5, and then dropped to 14.51% at La/L=0.8. The similar trend of HHV of syngas was observed, which increased from 4.07 to 5.52 MJ/Nm^3 as La/L increased from 0.2 to 0.5, and then dropped to 4.64 MJ/Nm^3 at La/L=0.8. The results indicate that to achieve highest HHV of syngas, the air inlet should be located at the middle of the fixed-bed gasifier. To the best of authors' knowledge,

there is no detailed experimental data being reported to show how the air inlet location affects the syngas composition. However, a rough guideline about the geometry design was provided by Albrecht Kaupp [75], who concluded that downdraft gasifiers with middle air inlet are preferred and this type of gasifier has been most extensively studied.

The effects of air inlet location on biochar production is shown in **Figure 8b**. The production rate of biochar and its carbon content decreased from 21.19% to 19.26% kg/kg feedstock and from 87.13% to 84.32% as La/L increased from 0.2 to 0.5, respectively. As La/L increased from 0.5 to 0.8, the production rate of biochar and its carbon content increased from 19.26% to 19.37% kg/kg feedstock and from 84.32% to 84.51%, respectively. Since the residence time and ER remain constant, the biochar production is only affected by the temperature profile inside the reactor, which is shown in **Figure 8c**. Biomass particles enter the reactor with room temperature and it will undergo heterogeneous reactions and be preheated before reaching the mixed convection region. In the cases of La/L=0.2, La/L=0.3, and La/L=0.4, biomass particles reach the mixed convection region (where the air inlets locate) without being fully preheated, thus peak temperatures were lowered down, which would further lead to the lower temperature profiles in other regions. Heterogeneous reactions are slowed down due to lower temperature. That's why the production rate of biochar and its carbon content decreased as La/L increased from 0.2 to 0.5. As La/L increased from 0.5 to 0.8, peak temperature remains constant, while biomass particles stay longer time in the lower temperature region. This leads to the increases of the production rate of biochar and its carbon content as La/L increased from 0.5 to 0.8.

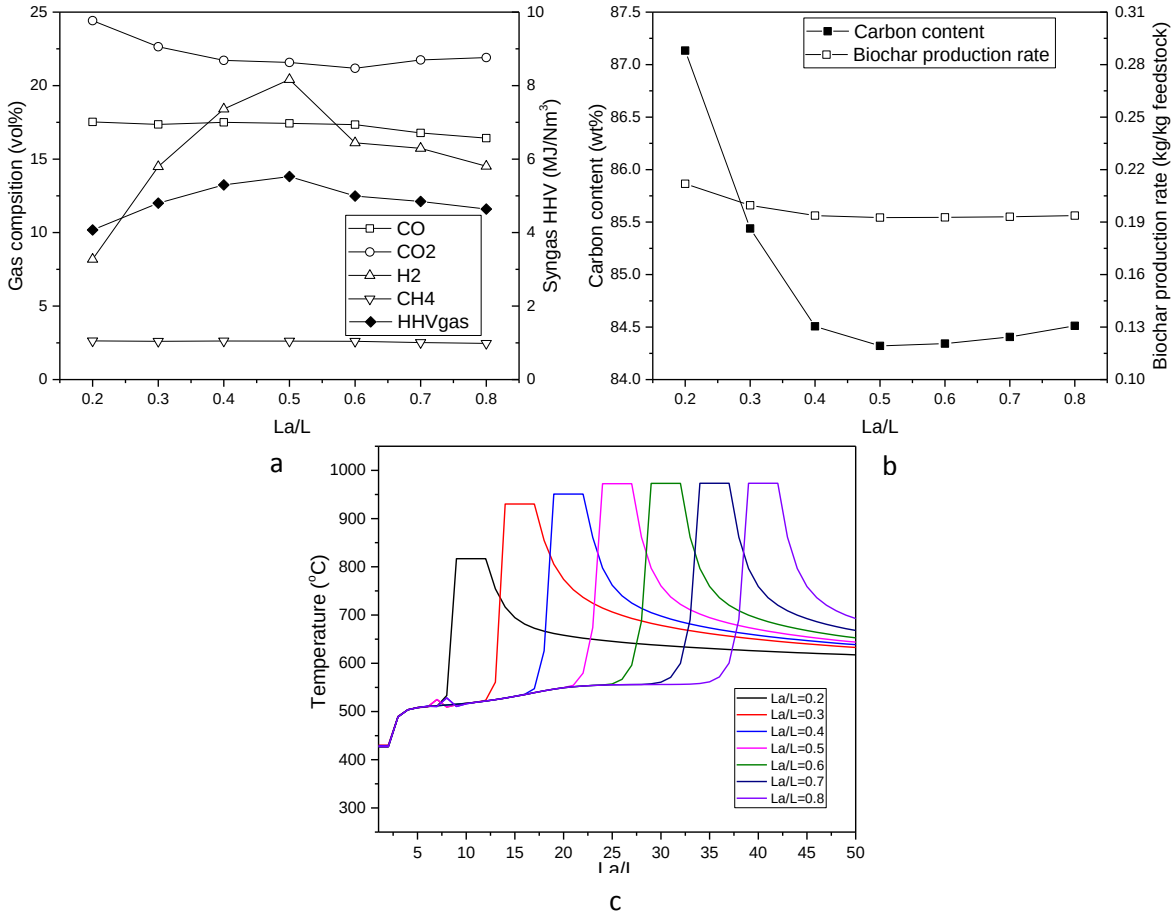

Figure 8a; Effects of air inlet location on syngas composition;
Figure 8b: Effects of air inlet location on biochar production and its carbon content;
Figure 8c: Temperature profile under different air inlet locations.

5 Conclusions

In this study, a coupled transient single particle and fix-bed model is developed to describe the entire packed bed in the flow direction of primary air. In this model, a three-region approach is applied to simulate heat and mass transfer inside the reactor based on different gas velocity profiles. The model has the capacity to predict the production rate and quality of both syngas and biochar produced from the gasification process. The results predicted by the model agree well with experimental results and the SDs between the numerical and experimental results obtained in this study are lower than 10%. The model is applicable for analysis of fixed-bed biomass gasification process under different operating conditions in terms of ER, the moisture content of feedstock, and air inlet location. By considering the

contributions of both syngas and biochar, the optimum ER was found to be 0.25 in terms of economic benefits of the gasification process. The maximum economic benefit could reach 0.11 $/kg feedstock based on the model prediction.

Acknowledgements

This research programme is funded by the National Research Foundation (NRF), Prime Minister's Office, Singapore under its Campus for Research Excellence and Technological Enterprise (CREATE) programme. Grant Number R- 706-001-101–281, National University of Singapore. The authors acknowledge the technical support of Yan Wei-Cheng on the project.

Nomenclature

A	Cross sectional area of the bed	m^2
A_v	specific surface area	m^{-1}
cp	specific heat capacity	$J\ kg^{-1}K^{-1}$
D	diffusivity	$m^2\ s^{-1}$
d	diameter	m
F	mass flow rate	$kg\ s^{-1}$
f_1	first frictional factor	$kg\ m^{-3}s^{-1}$
f_2	second frictional factor	$kg\ m^{-4}$
G	gas mass flux	$kg\ m^{-2}s^{-1}$
ΔH	enthalpy change	$J\ mol^{-1}$
h	heat transfer coefficient	$W\ m^{-2}K^{-1}$
k	mass transfer coefficient	$m\ s^{-1}$
L	reactor length in axial direction	m
L^*	characteristic length	m
M	molecular weight	$kg\ mol^{-1}$

Nu	Nusselt number	-
q	heat flux	W m^{-2}
R	gas constant	8.314 J mol^{-1} K^{-1}
RM	removing rate	kg s^{-1}
Re	Reynolds number	-
r_{vol}	volume reaction rate	mol $m^{-3}s^{-1}$
r_{suf}	surface reaction rate	mol $m^{-2}s^{-1}$
Sc	Schmidt number	-
Sh	Sherwood number	-
s_k	film diffusion rate	m s^{-1}
T	temperature	K
t	time	s
u	velocity	m s^{-1}
Y	mass fraction	-

Greek letters

ε	porosity	-
ρ	density	kg m^{-3}
υ	stoichiometric number	-
μ	effective viscosity	kg $m^{-1}s^{-1}$
β	fluid coefficient of thermal expansion	K^{-1}
η	dynamic viscosity	Pa s^{-1}
ϵ_t	turbulent dissipation rate	m^2 s^{-3}
ϵ	particle emissivity	-
σ	Stefan–Boltzmann constant	5.67×10^{-8} W $m^{-2}K^{-4}$
κ	thermal conductivity	W $m^{-1}K^{-1}$

Subscripts

a	The region above air inlet location

b	fixed bed
des	desorption
f	forced convection region
g	pertains to gas phase
gs	heat or mass transfer between gas phase and solid phase
in	air inlet
i	pertains to specie or component in gas phase with index i
j	pertains to specie or component in solid phase with index j
k	pertains to reaction number with index k
m	mixed convection
n	natural convection
s	pertains to solid phase
sat	saturation
ss	heat or mass transfer in solid phase
suf	surface
tm	turbulent mixing
vap	vaporization
vol	volume
w	water

A	Cross sectional area of the bed	m^2
A_v	specific surface area	m^{-1}
c_p	specific heat capacity	$J\ kg^{-1}K^{-1}$
D	diffusivity	$m^2\ s^{-1}$
d	diameter	m
F	mass flow rate	$kg\ s^{-1}$
f_1	first frictional factor	$kg\ m^{-3}s^{-1}$
f_2	second frictional factor	$kg\ m^{-4}$

G	gas mass flux	kg $m^{-2}s^{-1}$
ΔH	enthalpy change	J mol^{-1}
h	heat transfer coefficient	W $m^{-2}K^{-1}$
k	mass transfer coefficient	m s^{-1}
L	reactor length in axial direction	m
L^*	characteristic length	m
M	molecular weight	kg mol^{-1}
Nu	Nusselt number	-
q	heat flux	W m^{-2}
R	reaction rate	mol $m^{-3}s^{-1}$
RM	removing rate	kg s^{-1}
Re	Reynolds number	-
r_{vol}	volume reaction rate	mol $m^{-3}s^{-1}$
r_{suf}	surface reaction rate	mol $m^{-2}s^{-1}$
Sc	Schmidt number	-
Sh	Sherwood number	-
s_k	film diffusion rate	kg $m^{-2}s^{-1}$
T	temperature	K
t	time	s
u	velocity	m s^{-1}
Y	mass fraction	-

Greek letters

ε	porosity	-
ρ	density	kg m^{-3}
υ	stoichiometric number	-
μ	effective viscosity	kg $m^{-1}s^{-1}$
β	fluid coefficient of thermal expansion	K^{-1}
η	dynamic viscosity	Pa s^{-1}

ϵ_t	turbulent dissipation rate	$m^2\ s^{-3}$
ϵ	particle emissivity	-
σ	Stefan–Boltzmann constant	$W\ m^{-2}K^{-4}$
κ	thermal conductivity	$W\ m^{-1}K^{-1}$

Subscripts

a	The region above air inlet location
b	fixed bed
des	desorption
f	forced convection region
g	pertains to gas phase
gs	heat or mass transfer between gas phase and solid phase
in	air inlet
i	pertains to specie or component in gas phase with index i
j	pertains to specie or component in solid phase with index j
k	pertains to reaction number with index k
m	mixed convection
n	natural convection
s	pertains to solid phase
sat	saturation
ss	heat or mass transfer in solid phase
suf	pertains to surface reactions
tm	turbulent mixing
vap	vaporization
vol	volume to volume reactions
w	water

Reference

[1] Knoef H, Ahrenfeldt J. Handbook biomass gasification: BTG biomass technology group The Netherlands; 2005.

[2] Ngo SI, Nguyen TDB, Lim Y-I, Song B-H, Lee U-D, Choi Y-T, et al. Performance evaluation for dual circulating fluidized-bed steam gasifier of biomass using quasi-equilibrium three-stage gasification model. Applied Energy. 2011;88:5208-20.

[3] Janajreh I, Al Shrah M. Numerical and experimental investigation of downdraft gasification of wood chips. Energy Conversion and Management. 2013;65:783-92.

[4] You S, Wang W, Dai Y, Tong YW, Wang CH. Comparison of the co-gasification of sewage sludge and food wastes and cost-benefit analysis of gasification- and incineration-based waste treatment schemes. Bioresour Technol. 2016;218:595-605.

[5] Bridgwater AV. Renewable fuels and chemicals by thermal processing of biomass. Chemical Engineering Journal. 2003;91:87-102.

[6] Reed T, Das A. Handbook of biomass downdraft gasifier engine systems: Biomass Energy Foundation; 1988.

[7] Gambarotta A, Morini M, Zubani A. A non-stoichiometric equilibrium model for the simulation of the biomass gasification process. Applied Energy. 2017.

[8] Di Blasi C. Dynamic behaviour of stratified downdraft gasifiers. Chemical engineering science. 2000;55:2931-44.

[9] Babu B, Sheth PN. Modeling and simulation of reduction zone of downdraft biomass gasifier: effect of char reactivity factor. Energy Conversion and Management. 2006;47:2602-11.

[10] Gao N, Li A. Modeling and simulation of combined pyrolysis and reduction zone for a downdraft biomass gasifier. Energy Conversion and Management. 2008;49:3483-90.

[11] Ong Z, Cheng Y, Maneerung T, Yao Z, Tong YW, Wang C-H, et al. Co-gasification of woody biomass and sewage sludge in a fixed-bed downdraft gasifier. AIChE Journal. 2015;61:2508-21.

[12] Wu Y, Zhang Q, Yang W, Blasiak W. Two-dimensional computational fluid dynamics simulation of biomass gasification in a downdraft fixed-bed gasifier with highly preheated air and steam. Energy & Fuels. 2013;27:3274-82.

[13] Ahmed TY, Ahmad MM, Yusup S, Inayat A, Khan Z. Mathematical and computational approaches for design of biomass gasification for hydrogen production: A review. Renewable and Sustainable Energy Reviews. 2012;16:2304-15.

[14] He C, Feng X, Chu KH. Process modeling and thermodynamic analysis of Lurgi fixed-bed coal gasifier in an SNG plant. Applied Energy. 2013;111:742-57.

[15] Baruah D, Baruah DC, Hazarika MK. Artificial neural network based modeling of biomass gasification in fixed bed downdraft gasifiers. Biomass and Bioenergy. 2017;98:264-71.

[16] Mikulandrić R, Böhning D, Böhme R, Helsen L, Beckmann M, Lončar D. Dynamic modelling of biomass gasification in a co-current fixed bed gasifier. Energy Conversion and Management. 2016;125:264-76.

[17] Maneerung T, Liew J, Dai Y, Kawi S, Chong C, Wang CH. Activated carbon derived from carbon residue from biomass gasification and its application for dye adsorption: Kinetics, isotherms and thermodynamic studies. Bioresour Technol. 2016;200:350-9.

[18] Ng WC, You S, Ling R, Gin KY-H, Dai Y, Wang C-H. Co-gasification of woody biomass and chicken manure: Syngas production, biochar reutilization, and cost-benefit analysis. Energy. 2017;139:732-42.

[19] You S, Ok YS, Chen SS, Tsang DC, Kwon EE, Lee J, et al. A Critical Review on Sustainable Biochar System through Gasification: Energy and Environmental Applications. Bioresource Technology. 2017.

[20] Anca-Couce A, Zobel N, Jakobsen HA. Multi-scale modeling of fixed-bed thermo-chemical processes of biomass with the representative particle model: Application to pyrolysis. Fuel. 2013;103:773-82.

[21] Di Blasi C. Modeling chemical and physical processes of wood and biomass pyrolysis. Progress in Energy and Combustion Science. 2008;34:47-90.
[22] Lerou JJ, Ng KM. Chemical reaction engineering: A multiscale approach to a multiobjective task. Chemical Engineering Science. 1996;51:1595-614.
[23] Peters B. Measurements and application of a discrete particle model (DPM) to simulate combustion of a packed bed of individual fuel particles. Combustion and Flame. 2002;131:132-46.
[24] Johansson R, Thunman H, Leckner B. Influence of intraparticle gradients in modeling of fixed bed combustion. Combustion and Flame. 2007;149:49-62.
[25] Peters B, Schröder E, Bruch C. Measurements and particle resolved modelling of the thermo-and fluid dynamics of a packed bed. Journal of Analytical and Applied Pyrolysis. 2003;70:211-31.
[26] Gupta P, Sadhukhan AK, Saha RK. Analysis of the combustion reaction of carbon and lignite char with ignition and extinction phenomena: Shrinking sphere model. International Journal of Chemical Kinetics. 2007;39:307-19.
[27] Sadhukhan AK, Gupta P, Saha RK. Analysis of the dynamics of coal char combustion with ignition and extinction phenomena: shrinking core model. International Journal of Chemical Kinetics. 2008;40:569-82.
[28] Wurzenberger J. A combined packed bed and single particle model applied to biomass combustion: na; 2001.
[29] Wurzenberger JC, Wallner S, Raupenstrauch H, Khinast JG. Thermal conversion of biomass: Comprehensive reactor and particle modeling. AIChE Journal. 2002;48:2398-411.
[30] Porteiro J, Collazo J, Patino D, Granada E, Moran Gonzalez JC, Míguez JLs. Numerical modeling of a biomass pellet domestic boiler. Energy & Fuels. 2009;23:1067-75.
[31] Cengel YA, Ghajar A. Heat and mass transfer (a practical approach, SI version). McGraw-Hill Education; 2011.
[32] Nithiarasu P, Seetharamu K, Sundararajan T. Natural convective heat transfer in a fluid saturated variable porosity medium. International Journal of Heat and Mass Transfer. 1997;40:3955-67.
[33] Whitaker S. Forced convection heat transfer correlations for flow in pipes, past flat plates, single cylinders, single spheres, and for flow in packed beds and tube bundles. AIChE Journal. 1972;18:361-71.
[34] Chen C-H, Chen T, Cha O, Chen K. Non-Darcy mixed convection along nonisothermal vertical surfaces in porous media. International journal of heat and mass transfer. 1996;39:1157-64.
[35] Pop I, Ingham DB. Transport Phenomena in Porous Media II: Elsevier; 2002.
[36] Zobel N. The representative particle model2007.
[37] Abbas MN. Modeling of porosity equation for water flow through packed bed Of monosize spherical packing. Journal of engineering and development. 2011;15.
[38] Khiari B, Marias F, Vaxelaire J, Zagrouba F. Incineration of a small particle of wet sewage sludge: A numerical comparison between two states of the surrounding atmosphere. Journal of hazardous materials. 2007;147:871-82.
[39] Donaj P, Izadpanah MR, Yang W, Blasiak W. Effect of pressure drop due to grate–bed resistance on the performance of a downdraft gasifier. Energy & Fuels. 2011;25:5366-77.
[40] Di Blasi C, Signorelli G, Di Russo C, Rea G. Product distribution from pyrolysis of wood and agricultural residues. Industrial & Engineering Chemistry Research. 1999;38:2216-24.
[41] Boroson ML, Howard JB, Longwell JP, Peters WA. Product yields and kinetics from the vapor phase cracking of wood pyrolysis tars. AIChE Journal. 1989;35:120-8.
[42] Hobbs ML, Radulovic PT, Smoot LD. Modeling fixed - bed coal gasifiers. AIChE Journal. 1992;38:681-702.
[43] Hobbs M, Radulovic P, Smoot L. Combustion and gasification of coals in fixed-beds. Progress in Energy and Combustion Science. 1993;19:505-86.
[44] Arthur J. Reactions between carbon and oxygen. Transactions of the Faraday Society. 1951;47:164-78.

[45] Yoon H, Wei J, Denn MM. A model for moving‐bed coal gasification reactors. AIChE Journal. 1978;24:885-903.
[46] Siminski V, Wright F, Edelman R, Economos C, Fortune O. Research on methods of improving the combustion characteristics of liquid hydrocarbon fuels. Report AFAPLTR. 1972:72-4.
[47] Gerber S, Behrendt F, Oevermann M. An Eulerian modeling approach of wood gasification in a bubbling fluidized bed reactor using char as bed material. Fuel. 2010;89:2903-17.
[48] Varma AK, Chatwani AU, Bracco FV. Studies of premixed laminar hydrogen・air flames using elementary and global kinetics models. Combustion and flame. 1986;64:233-6.
[49] Howard J, Williams G, Fine D. Kinetics of carbon monoxide oxidation in postflame gases. Symposium (International) on Combustion: Elsevier; 1973. p. 975-86.
[50] Macak J, Malecha J. Mathematical model for the gasification of coal under pressure. Industrial & Engineering Chemistry Process Design and Development. 1978;17:92-8.
[51] Dryer F, Glassman I. High-temperature oxidation of CO and CH4. Symposium (International) on combustion: Elsevier; 1973. p. 987-1003.
[52] Jones W, Lindstedt R. Global reaction schemes for hydrocarbon combustion. Combustion and flame. 1988;73:233-49.
[53] Wakao N, Kagei S. Heat and mass transfer in packed beds: Taylor & Francis; 1982.
[54] Ferziger JH, Peric M. Computational methods for fluid dynamics: Springer Science & Business Media; 2012.
[55] Jakobsen HA, Lindborg H, Handeland V. A numerical study of the interactions between viscous flow, transport and kinetics in fixed bed reactors. Computers & chemical engineering. 2002;26:333-57.
[56] Lindborg H, Eide V, Unger S, Henriksen ST, Jakobsen HA. Parallelization and performance optimization of a dynamic PDE fixed bed reactor model for practical applications. Computers & chemical engineering. 2004;28:1585-97.
[57] Oevermann M, Gerber S, Behrendt F. Euler–Lagrange/DEM simulation of wood gasification in a bubbling fluidized bed reactor. Particuology. 2009;7:307-16.
[58] McBride BJ, Gordon S, Reno MA. Coefficients for calculating thermodynamic and transport properties of individual species. 1993.
[59] Welty JR, Wicks CE, Rorrer G, Wilson RE. Fundamentals of momentum, heat, and mass transfer: John Wiley & Sons; 2009.
[60] Pinto F, André RN, Lopes H, Dias M, Gulyurtlu I, Cabrita I. Effect of experimental conditions on gas quality and solids produced by sewage sludge cogasification. 2. Sewage sludge mixed with biomass. Energy & Fuels. 2008;22:2314-25.
[61] Sheth PN, Babu B. Experimental studies on producer gas generation from wood waste in a downdraft biomass gasifier. Bioresource Technology. 2009;100:3127-33.
[62] Channiwala S, Parikh P. A unified correlation for estimating HHV of solid, liquid and gaseous fuels. Fuel. 2002;81:1051-63.
[63] Yoder J, Galinato S, Granatstein D, Garcia-Pérez M. Economic tradeoff between biochar and bio-oil production via pyrolysis. biomass and bioenergy. 2011;35:1851-62.
[64] Wang J, Mao T, Sui J, Jin H. Modeling and performance analysis of CCHP (combined cooling, heating and power) system based on co-firing of natural gas and biomass gasification gas. Energy. 2015;93:801-15.
[65] Lv P, Xiong Z, Chang J, Wu C, Chen Y, Zhu J. An experimental study on biomass air–steam gasification in a fluidized bed. Bioresource technology. 2004;95:95-101.
[66] Mahishi MR, Goswami D. Thermodynamic optimization of biomass gasifier for hydrogen production. International Journal of Hydrogen Energy. 2007;32:3831-40.
[67] Seggiani M, Puccini M, Raggio G, Vitolo S. Effect of sewage sludge content on gas quality and solid residues produced by cogasification in an updraft gasifier. Waste management. 2012;32:1826-34.

[68] Dogru M, Howarth C, Akay G, Keskinler B, Malik A. Gasification of hazelnut shells in a downdraft gasifier. Energy. 2002;27:415-27.
[69] Zainal Z, Rifau A, Quadir G, Seetharamu K. Experimental investigation of a downdraft biomass gasifier. Biomass and bioenergy. 2002;23:283-9.
[70] Zainal Z, Ali R, Lean C, Seetharamu K. Prediction of performance of a downdraft gasifier using equilibrium modeling for different biomass materials. Energy conversion and management. 2001;42:1499-515.
[71] Meyer S, Glaser B, Quicker P. Technical, economical, and climate-related aspects of biochar production technologies: a literature review. Environ Sci Technol. 2011;45:9473-83.
[72] Yang Z, Koh SK, Ng WC, Lim RC, Tan HT, Tong YW, et al. Potential application of gasification to recycle food waste and rehabilitate acidic soil from secondary forests on degraded land in Southeast Asia. Journal of environmental management. 2016;172:40-8.
[73] Shackley S, Ibarrola Esteinou, R., Hopkins, D., & Hammond, J. Biochar Quality Mandate (BQM) version 1.0. British Biochar Foundation. 2014.
[74] Xie L-P, Tao L, Gao J-D, Fei X-N, Xia W, Jiang Y-G. Effect of moisture content in sewage sludge on air gasification. Journal of Fuel Chemistry and Technology. 2010;38:615-20.
[75] Kaupp A. Small scale gas producer-engine systems: Springer Science & Business Media; 2013.